Periodic solutions of pendulum: II

2003 J. Phys. A: Math. Gen. 36 6691

(http://iopscience.iop.org/0305-4470/36/24/308)

INSTITUTE OF PHYSICS PUBLISHING JOURNAL OF PHYSICS A: MATHEMATICAL AND GENERAL

J. Phys. A: Math. Gen. **36** (2003) 6691–6707 PII: S0305-4470(03)57013-5

Periodic solutions of pendulum: II

M Y Kucinski[1] **and L H A Monteiro**[2,3]

[1] Instituto de Física da Universidade de São Paulo, rua do Matão - trav R, 187, CEP 05508-900 São Paulo, SP, Brazil
[2] Universidade Presbiteriana Mackenzie, Pós-graduação – Engenharia Elétrica, Rua da Consolação, 896, edifício Amantino Vassão, térreo, CEP 01302-907 São Paulo, SP, Brazil
[3] Universidade de São Paulo, Escola Politécnica, Departamento de Engenharia de Telecomunicações e Controle, Av. Prof. Luciano Gualberto, travessa 3, n.380, CEP 05508-900 São Paulo, SP, Brazil

E-mail: mkucinsk@if.usp.br and luizm@mackenzie.com.br

Received 2 December 2002, in final form 8 April 2003
Published 5 June 2003
Online at stacks.iop.org/JPhysA/36/6691

Abstract

Period-3 oscillations of pendulum are investigated using the method developed in our previous paper [1]. Values of the driving force within very narrow ranges may give rise to this kind of motion. Because of the extreme sensitivity of the equation to the force strength and initial conditions, some features of the system can hardly be depicted, either numerically or experimentally. However, by analytically obtaining a map of states it is possible to detect the underlying structure of the system of solutions. The theory predicts the existence of unstable periodic solutions. Also, it predicts stable period-3 solutions around the top position of pendulum. Trajectories obtained by numerically integrating the pendulum equation in a phase-locked condition agree with our diagrams.

PACS numbers: 05.45.−a, 45.50.−j

1. Introduction

The motion of a harmonically driven, linear damped pendulum in a gravitational field obeys the differential equation

$$\ddot{\theta} + \sigma\dot{\theta} + (\omega_0)^2 \sin\theta = A \sin\omega_d\tau \tag{1.1}$$

where θ is the angular displacement from the vertical resting axis at time τ, ω_0 is the undamped natural frequency for small-amplitude oscillations, ω_d is the frequency of the external driving, and σ and A are the damping constant and the amplitude of the driving, respectively, in appropriate units. The dot means derivation with respect to τ. In dimensionless form, this equation can be rewritten as

$$f^2\ddot{\theta} + \epsilon f\dot{\theta} + \sin\theta = a \sin t \tag{1.2}$$

where $f \equiv \omega_d/\omega_0, \epsilon \equiv \sigma/\omega_0, a \equiv A/(w_0)^2$ and $t \equiv \omega_d\tau$. The dot now means derivation with respect to t.

A harmonically driven pendulum can exhibit periodic motion. Phase-locking occurs when the oscillation frequency of the motion is a rational multiple of the frequency ω_d of the driving torque. In these cases drive and damping exactly balance in one cycle.

If the amplitude a of the driving term is small, we expect, on physical grounds, mode-locked orbits where the pendulum oscillates at the frequency of the driving force. These orbits are period-1 limit cycles in the phase space. However, if the amplitude of the drive is increased, we can expect to see limit cycles with periods other than 1 due to the nonlinear nature of the system. The system behaviour is usually examined by drawing the phase diagrams obtained by numerical integration of equation (1.2).

In the paper [1] an analytical procedure is developed for determining phase diagrams for a pendulum described by (1.2). The results for period-1 solution were successfully compared to those obtained by numerically integrating such an equation.

Here, we deal with the period-3 solution. This behaviour has been found in experimental works with mechanical pendulums [2] and analogue electronic circuits [3], and in computer simulations [4–6].

The results discussed here are all for the case $f = 0.689$ and $\epsilon = 0.2$ for the simple reason that Rasband [7] found, numerically, a period-3 motion using these values.

The main ideas of the theory are exposed in our previous paper. Hereafter we call it paper I. The derivation of the formulae is not reproduced here. Also, the notation used here for the variables is basically the same as introduced in paper I.

The main formulae are written in a slightly different form in section 2. In section 3, an iterative method is established in order to solve the equations for period-3 motions. The numerical solutions are examined graphically in the phase space. In sections 4 and 5 we discuss our findings.

2. Period-3 solutions

Periodic solutions of (1.2) are represented by a Fourier series in the form

$$\theta = \Theta_0 + \sum_{m=1}^{\infty} C_m \sin\left(\frac{m}{p}t - \delta_m\right) \tag{2.1}$$

where p is an integer number with the meaning of oscillation period relative to driving period. For oscillation period equal to three times the driving period, p is 3. Θ_0 is the average position and C_m and δ_m are constants representing, respectively, the amplitude and phase of the harmonic oscillation with frequency m/p.

The value of θ is not necessarily in the interval $(-\pi, +\pi)$. Here θ is considered as the gyration angle in a vertical plane starting from the pendulum equilibrium position rather than the oscillation angle. Thus, if θ increases from 0 to 7 and then keeps oscillating in the interval $(-7, 7)$, this means that the pendulum rotates once in one direction before stopping, and then the motion is reversed and the pendulum rotates twice between two successive reversions.

By introducing

$$t_1 \equiv 3\delta_1 \qquad \text{and} \qquad \beta_m \equiv m\delta_1 - \delta_m \quad m \geqslant 1$$

in (2.1), we get

$$\theta = \Theta_0 + \sum_{m=1}^{\infty} C_m \sin\left(\frac{m}{3}(t - t_1) + \beta_m\right). \tag{2.2}$$

It is clear in this equation that the main features of the motion do not effectively depend on the values of all parameters δ_m; $t_1 \equiv 3\delta_1$ just represents a time shift. β_m is the phase shift of each harmonic and it is relevant for the description of the behaviour of the pendulum. We recall that $\beta_1 = 0$.

The system of equations to determine C_m and δ_m (or β_m) is obtained by using

$$\sum \ell_m \delta_m = \sum \ell_m(\delta_m - m\delta_1) + \sum \ell_m m\delta_1 = -\sum \ell_m \beta_m + s\delta_1 = -\sum \ell_m \beta_m + \beta_s + \delta_s$$

in equations (2.4), (2.9) and (2.11) of paper I.

Nonoscillatory term ($s = 0$)

$$\sin\Theta_0 \sum_{\ell_t=\text{even}}^{0} J_{\ell_1}(C_1)J_{\ell_2}(C_2)\cdots \cos\left(\sum_{m=1}^{\infty} \ell_m\beta_m\right) + \cos\Theta_0 \sum_{\ell_t=\text{odd}}^{0} J_{\ell_1}(C_1)J_{\ell_2}(C_2)\cdots \sin\left(\sum_{m=1}^{\infty} \ell_m\beta_m\right) = 0. \tag{2.3}$$

Harmonic 3

$$(-f^2 + \mathrm{i}\epsilon f)C_3 + 2\cos\Theta_0 j_3(C)J_1(C_3) = a\,\mathrm{e}^{\mathrm{i}\delta_3} + d_3(C,\beta)\,\mathrm{e}^{-\mathrm{i}\beta_3}. \tag{2.4}$$

$j_3(C)$ is the product of all 0-order Bessel functions but $J_0(C_3)$:

$$j_3(C) \equiv J_0(C_1)J_0(C_2)J_0(C_4)\cdots J_0(C_m)\cdots \tag{2.5}$$

and

$$-d_3(C,\beta) \equiv 2\mathrm{i}\sin\Theta_0 \sum_{\ell_t=\text{even}}^{3} J^{\ell_t}\,\mathrm{e}^{+\mathrm{i}\sum \ell_m\beta_m} + 2\cos\Theta_0\left(\sum_{\ell_t=\text{odd}}^{3} J^{\ell_t}\,\mathrm{e}^{+\mathrm{i}\sum \ell_m\beta_m} - j_3(C)J_1(C_3)\,\mathrm{e}^{\mathrm{i}\beta_3}\right) \tag{2.6}$$

$C \equiv \{C_1, C_2, C_3, \ldots\}$ and $\beta \equiv \{\beta_1, \beta_2, \beta_3, \ldots\}$.

Harmonic $s \neq 0$ and 3

$$\left(-\left(\frac{fs}{3}\right)^2 + \mathrm{i}\epsilon\frac{fs}{3}\right)C_s + 2\cos\Theta_0 j_s(C)J_1(C_s) = d_s(C,\beta)\,\mathrm{e}^{-\mathrm{i}\beta_s} \tag{2.7}$$

with

$$-d_s(C,\beta) \equiv 2\mathrm{i}\sin\Theta_0 \sum_{\ell_t=\text{even}}^{s} J^{\ell_t}\,\mathrm{e}^{+\mathrm{i}\sum \ell_m\beta_m} + 2\cos\Theta_0\left(\sum_{\ell_t=\text{odd}}^{s} J^{\ell_t}\,\mathrm{e}^{+\mathrm{i}\sum \ell_m\beta_m} - j_s(C)J_1(C_s)\,\mathrm{e}^{+\mathrm{i}\beta_s}\right). \tag{2.8}$$

Here,

$$\ell_t \equiv \sum_{m=1}^{\infty} \ell_m \qquad J^{\ell_t} \equiv J_{\ell_1}(C_1)J_{\ell_2}(C_2)\cdots$$

and

$$\sum_{\ell_t=\text{even}}^{s}$$

is the sum over all possible values of $\{\ell_1, \ell_2, \ldots\}$ that satisfy $\ell_1 + 2\ell_2 + 3\ell_3 + \cdots = s$ and $\ell_t =$ even number.

2.1. Assumptions

C_3 is the amplitude of oscillation with the frequency of the driving force. We consider here stationary solutions with frequency of oscillation equal to one-third of the frequency of the driving force; C_1 is the amplitude of the fundamental oscillation. Therefore, we assume that these two coefficients are hierarchically more relevant than the others.

Moreover, as we search for convergent Fourier series, we assume that C_j is negligible for $j > M$. If $C_j = 0$, then $J_{\ell_j}(C_j) = 0$ unless $\ell_j = 0$. $J_0(0) = 1$.

It is a well known property of Bessel functions that $\lim_{k\to\infty} J_k(C_j) = 0$. We assume that $J_{\ell_j}(C_j)$ is negligible for $|\ell_j| > \ell_{j\max}$.

Thus, we take $|\ell_j| = 0$ for $j > M$ and $|\ell_j| \leqslant \ell_{j\max}$ for $j \leqslant M$.

We found that for $M = 13$ the agreement between the analytical and the numerical orbits in the phase diagram is almost perfect. The neglected coefficients are found to be smaller than 1% of C_1 or C_3 in all cases. In some cases they were much smaller.

We can describe the main dynamic features with fewer coefficients but we need very high accuracy in order to compare with the results of direct numerical integration of (1.2), as the equation may be very unstable.

2.2. Symmetric solutions

We call it symmetric if, in the second half period (of motion, not of the driving force), the pendulum is in the opposite position compared to the first half period, with respect to the average position $\theta = \Theta_0$, and moving in the opposite direction:

$$\theta(t + 3\pi) = -\theta(t) \qquad \text{and} \qquad \dot\theta(t + 3\pi) = -\dot\theta(t).$$

Therefore, if the solution is symmetric, all even order coefficients in the expression (2.2) are null.

If $C_2 = C_4 = \cdots = 0$, only terms $\ell_2 = \ell_4 = \cdots = 0$ are relevant. As

$$s \equiv \sum m\ell_m = \ell_t + (\ell_2 + 3\ell_4 + 5\ell_6 + \cdots) + (2\ell_3 + 4\ell_5 + 6\ell_7 + \cdots)$$

$$\text{parity of } s = \text{parity of } \ell_t + \text{parity of } \sum \ell_{2j} = \text{parity of } \ell_t.$$

In (2.3) ℓ_t must be an even number and therefore

$$\Theta_0 = 0 \qquad \text{or} \qquad \Theta_0 = \pi. \tag{2.9}$$

For $s =$ even number ($s = 2j$), (2.7) is reduced to

$$\left(-\left(\frac{f2j}{3}\right)^2 + \mathrm{i}\epsilon\frac{f2j}{3}\right) C_{2j} = 0 \tag{2.10}$$

with trivial solution $C_{2j} = 0$.

We assume, *a priori*, that C_{2j} is small and establish an iteration procedure starting with $C_{2j} = 0$. This method automatically yields symmetric solutions. We could possibly start with small but nonzero values of C_{2j} and see what we get. Fourier expansion of solutions obtained

by numerical integration of (1.2) was, most often, found with very small even order terms. As the numerical calculation is quite time consuming, we opted for addressing only this class of solutions.

3. Iteration method ($p = 3$ solutions)

Equation (2.4) is the only equation that explicitly contains a and δ_3. If instead of fixing a as a parameter, we choose some other variable, the system of equations becomes much more tractable, as (2.4) can be used to express a and δ_3 in terms of C_j and β_j. We choose to fix C_3 as a parameter.

Oscillations with average position $\Theta_0 = 0$ are thoroughly investigated here.

3.1. First order approximation

As a first order approximation, we consider

$$C_j = 0 \qquad \text{for} \qquad j \neq 1 \text{ and } 3. \tag{3.1}$$

3.1.1. C_1 and β_3. Equation (2.7) for $s = 1$ becomes

$$g(C_1, \beta_3) \equiv \left(-\left(\frac{f}{3}\right)^2 + \mathrm{i}\epsilon\frac{f}{3} \right) C_1 + 2\cos\Theta_0 \sum J_{\ell_1}(C_1) J_{\ell_3}(C_3)\, \mathrm{e}^{+\mathrm{i}\ell_3\beta_3} = 0 \tag{3.2}$$

where the $\sum$ is performed over all possible values of $\ell_1 \leqslant \ell_{1\max}$ and $\ell_3 \leqslant \ell_{3\max}$ that satisfy $\ell_1 + \ell_3 =$ odd and $\ell_1 + 3\ell_3 = 1$. C_3 is fixed as a parameter, as stated above.

This is a complex expression that can be written as two, real, implicit functions:

$$g_R(C_1, \beta_3) \equiv \mathrm{Re}(g(C_1, \beta_3)) = 0 \qquad \text{and} \qquad g_I(C_1, \beta_3) \equiv \mathrm{Im}(g(C_1, \beta_3)) = 0.$$

Here, Re and Im mean real and imaginary parts, respectively.

These functions are plotted in figure 1 for $\Theta_0 = 0$ for $C_3 < 3.5$. Full lines represent $g_R = 0$, and $g_I = 0$ is represented by broken lines. A continuous change of pattern occurs as C_3 is changed continuously.

For $C_1 < 8$ there are basically six groups of solutions (β_3, C_1) which we call **A, B, C, D, E** and **F**.

3.1.2. a and δ_3. Equation (2.4) becomes

$$\left(-f^2 + \mathrm{i}\epsilon f\right) C_3 + 2\cos\Theta_0 \sum J_{\ell_1}(C_1) J_{\ell_3}(C_3)\, \mathrm{e}^{+\mathrm{i}(\ell_1\beta_1 + (\ell_3 - 1)\beta_3)} = a\, \mathrm{e}^{\mathrm{i}\delta_3} \tag{3.3}$$

where ℓ_1 and ℓ_3 satisfy $\ell_1 + \ell_3 =$ odd and $\ell_1 + 3\ell_3 = 3$. a is the absolute value of the left-hand side of (3.3) and δ_3 is the argument of the same expression.

Alternatively, the energy balance equation

$$aC_3 \sin\delta_3 = \epsilon f \sum_{s=1}^{\infty} \left(\frac{sC_s}{3}\right)^2 \tag{3.4}$$

derived in paper I can be used to determine δ_3 in terms of a and other coefficients or, conversely, to find a in terms of δ_3 and the other parameters.

We call the values obtained for C_1, β_3, a and δ_3 first order solutions.

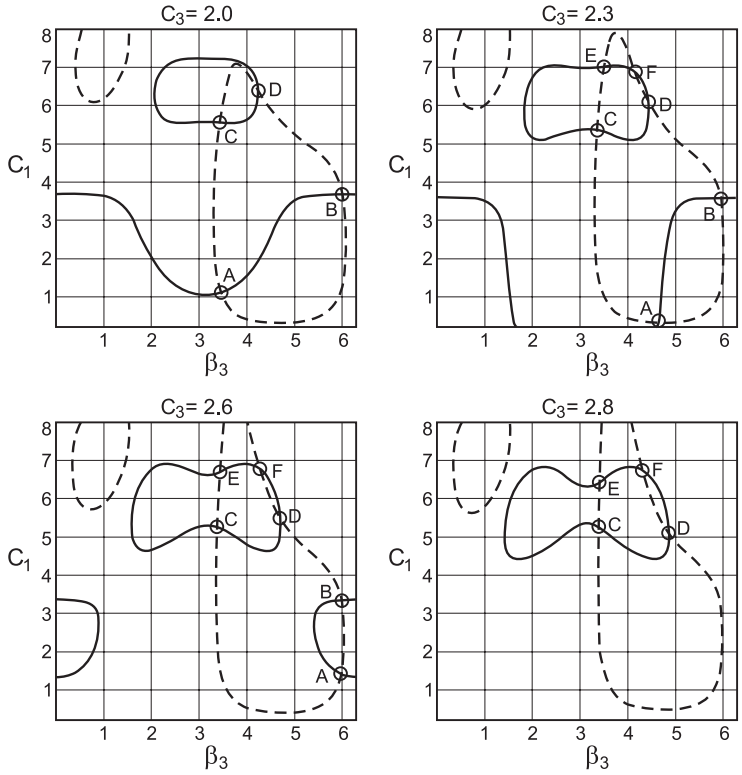

Figure 1. First order approximation. $\Theta_0 = 0$. For fixed C_3, $g_R(C_1, \beta_3) = 0$ is represented by full lines and $g_I(C_1, \beta_3) = 0$ is represented by broken lines. The values of C_1 and β_3 at the intersections are the first order solutions.

3.1.3. $\{C_s, \beta_s\}$; $s \geqslant 5$. C_5 and β_5 are determined by solving the equation

$$\left(-\left(\frac{5f}{3}\right)^2 + \mathrm{i}\epsilon\frac{5f}{3}\right) C_5 + 2\cos\Theta_0 j_5(C^0) J_1(C_5) = d_5(C^0, \beta^0)\,\mathrm{e}^{-\mathrm{i}\beta_3} \qquad (3.5)$$

where

$$C^0 \equiv \{C_1, C_3, \ldots, C_j^0, \ldots\} \qquad \text{and} \qquad \beta^0 \equiv \{0, \beta_3, \ldots, \beta_j^0, \ldots\}$$

with $C_j^0 = 0$ and $\beta_j^0 = 0$ for $j \geqslant 5$.

Analogously, we find $C_7, C_9, \ldots$ by using already known values for C^0 and β^0.

Phase paths of periodic motions surround either the lowest position of the pendulum (stable equilibrium point) or the top position (unstable equilibrium point).

3.2. Higher order approximation

Equation (2.7) is slightly modified to write for $s \neq 3$

$$\left(-\left(\frac{fs}{3}\right)^2 + \mathrm{i}\epsilon\frac{fs}{3}\right) C_s + 2\cos\Theta_0 j_s(C^0) J_1(C_s) = d_s(C^0, \beta^0)\,\mathrm{e}^{-\mathrm{i}\beta_3} \qquad (3.6)$$

where C^0 and β^0 are previously calculated values. As this is a complex function, it corresponds to two real equations and therefore it is enough to find C_s and β_s.

Equation (2.4) in the form

$$(-f^2 + \mathrm{i}\epsilon f)C_3 + 2\cos\Theta_0 j_3(C^0)J_1(C_3) = a\,\mathrm{e}^{\mathrm{i}\delta_3} + d_3(C^0, \beta^0)\,\mathrm{e}^{-\mathrm{i}\beta_3^0} \tag{3.7}$$

is used to find a and δ_3.

Once δ_3 and all coefficients C_s and β_s are found, we obtain

$$t_1 \equiv 3\delta_1 = \beta_3 + \delta_3 \qquad \text{and} \qquad \delta_s = \beta_s + s\delta_1.$$

δ_1 and all other δ_s are not uniquely defined (there must be three solutions) but the dynamic features described are the same.

The same procedure is repeated until the solution converges.

4. Results of numerical calculations

The major difficulty of this problem is that numerical integration of (1.2) requires very high accuracy; depending upon the values of the parameters, the equation may be unstable and then the solution strongly depends upon the initial conditions. The built-in function 'NDSolve' of the program 'MATHEMATICA' was used for this purpose, with options 'AccuracyGoal→ Infinity' and 'MaxSteps→ Infinity'. The integration was performed period by period in order to get maximum accuracy. By following this procedure, we found consistent results.

Moreover, a difference in the value of the driving a of less than 0.01% may produce completely different pictures. Therefore, analytically obtained C_j and a must be highly accurate in order to write the initial conditions and the corresponding differential equation that will be numerically integrated.

In the iteration method reported here, once C_3 is fixed, the phase portrait does not depend on the value of a as the equations for C_j and β_j, $j \neq 3$ do not contain a. a is related to the portrait through (2.4).

We take up to seven odd order coefficients and

$$\ell_{\max} \equiv \{\ell_{1\max}, \ell_{3\max}, \ldots, \ell_{13\max}\} = \{9, 7, 3, 1, 1, 1, 1\}$$

for oscillations centred in the stable equilibrium position $\Theta_0 = 0$ and

$$\ell_{\max} \equiv \{\ell_{1\max}, \ell_{3\max}, \ldots, \ell_{13\max}\} = \{7, 7, 3, 1, 1, 1, 1\}$$

for oscillations around the potential maximum of the pendulum, at $\Theta_0 = \pi$.

It is not necessary to take as many coefficients in order to get a reasonable picture but we need them to have reasonably accurate a. Iteration was performed until the values of C_1 and a converged to an accuracy of 10^{-6}. In most cases, more than ten iterations were necessary.

Also, (3.3) was used to find δ_3 and the energy balance equation (3.4) was used to determine a. The results differed by less than 0.1%.

We systematically adopted the following procedure:

- An orbit was found using this theory.
- Numerical integration of (1.2) was performed using one point of the analytical solution as initial conditions. The solutions were run through more than 180 periods of the driving force before drawing phase portraits.
- An equation with a slightly different value of a was numerically integrated starting from the same initial conditions.
- The same equation was integrated using different initial conditions in order to examine the stability of the orbit.
- When some interesting solutions were found by numerical integration, these solutions were Fourier decomposed, C_3 was found and then the theory was applied in order to compare the results.

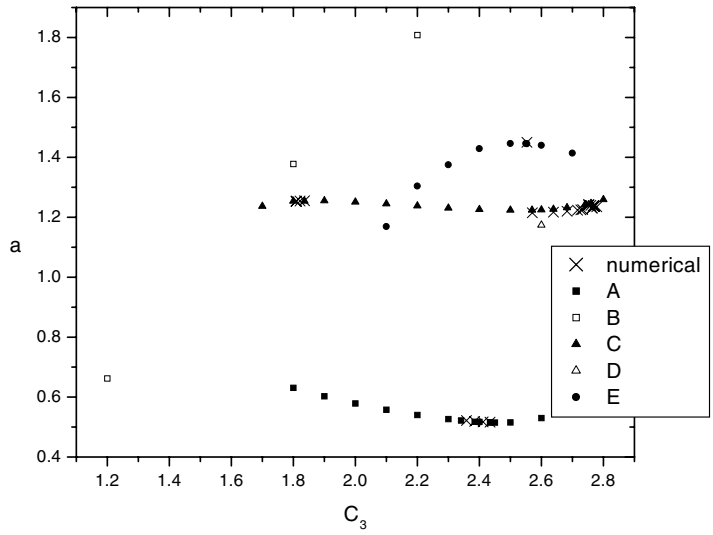

Figure 2. $\Theta_0 = 0$. All period-3 solutions found by the present method and by direct numerical integration of the differential equation for $f = 0.689$ and $\epsilon = 0.2$.

Motions centred in stable equilibrium position $\Theta_0 = 0$ were investigated with special care.

4.1. Case: $\Theta_0 = 0$

We restricted the values of C_3 and C_1 to the ranges $1.2 \leqslant C_3 \leqslant 3.6$ and $0.2 \leqslant C_1 \leqslant 8$.

Figure 2 shows all period-3 solutions found by our method and by direct numerical integration of the differential equation for $f = 0.689$ and $\epsilon = 0.2$.

4.1.1. Group A. Possible solutions in first order approximation are shown in figure 1. Each pair of values $\{C_1, \beta_3\}$, of the points **A, B, C, D, E** and **F**, corresponds to one orbit, due to driving a.

The method converged for $1.8 \leqslant C_3 \leqslant 2.6$. Figure 2 shows the convergent values of a and the results of numerical integration.

Period-3 orbits of type **A** were found numerically for $0.5153 \leqslant a \leqslant 0.521\,955$.

For values of a in this range, two attractors coexist: one with period 3 and another with period 1. Trajectories converge towards one of these attractors, as observed by Heng *et al* [6]. In fact, all solutions were highly dependent upon initial values.

For $a = 0.5232$ the period has been clearly duplicated. For $a = 0.525$ more complicated motion was obtained, seemingly chaotic; the trajectory remained well bounded in the phase space.

Outside this range of a, for $0.525 < a < 0.6$ and $a < 0.5153$, numerical integration always converged asymptotically to period-1 orbits.

A typical phase portrait, as found by Rasband [7], is shown in figure 3.

In the phase diagrams, $\{\theta(0), \dot{\theta}(0)\}$ are the initial values used for numerical integration. Full lines were obtained by numerical integration and the dots were obtained by using this theory. Odd order C_j and δ_j are given.

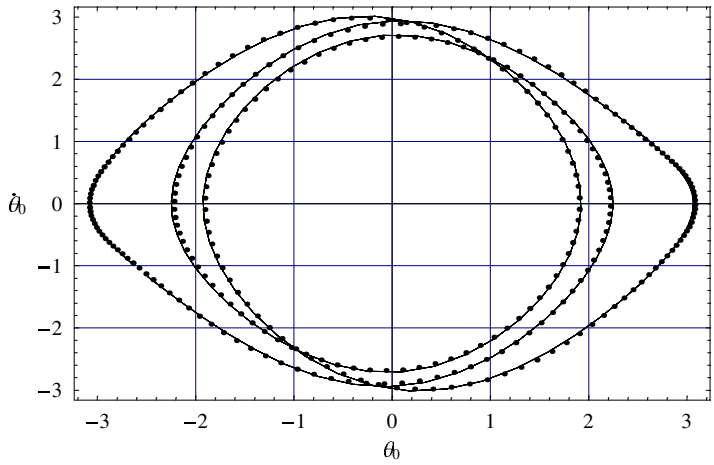

Figure 3. $a = 0.518\,57$, $\Theta_0 = 0$, $C = \{1.240\,78,\ 2.371\,88,\ 0.427\,24,\ 0.116\,823,\ 0.027\,744,\ 0.038\,342,\ 0.004\,487\}$, $\delta = \{2.063\,97,\ 2.342\,48,\ -0.479\,426,\ 0.658\,386,\ 0.174\,09,\ -1.959\,54,\ 0.167\,77\}$, $\{\theta(0), \dot{\theta}(0)\} = \{-2.637\,326\,4, -0.954\,636\,4\}$.

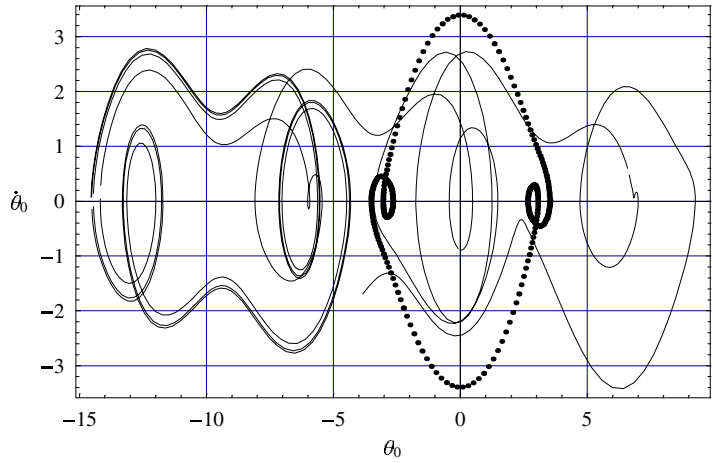

Figure 4. $a = 0.662\,5386$, $\Theta_0 = 0$, $C = \{3.762\,21, 1.2, 0.281\,255, 0.108\,206, 0.045\,335, 0.019\,424, 0.008\,593\}$, $\delta = \{2.832\,99,\ 2.527\,79,\ 1.718\,91,\ 1.209\,19,\ 0.687\,021,\ 0.186\,016,\ -0.340\,99\}$, $\{\theta(0), \dot{\theta}(0)\} = \{0, 0\}$.

4.1.2. Group B. The present method gave solutions for $1.2 \leqslant C_3 \leqslant 2.2$ (see figures 2, 4 and 5) but no orbit has been found by numerical integration. Numerical integration may converge to a solution centred on a maximum of the potential $\Theta_0 = \pi$ (figures 4, 5 and 15), indicating that the latter solution is certainly more stable.

4.1.3. Group C. Figure 2 is zoomed and shown as figure 6. Two sets of solutions were found by numerical integration:

- for $1.2533 \leqslant a \leqslant 1.255$ with $C_3 \simeq 1.82$ (figure 7);
- for $1.214\,87 \leqslant a \leqslant 1.243$ with $2.5709 \leqslant C_3 \leqslant 2.778\,57$ (figure 8).

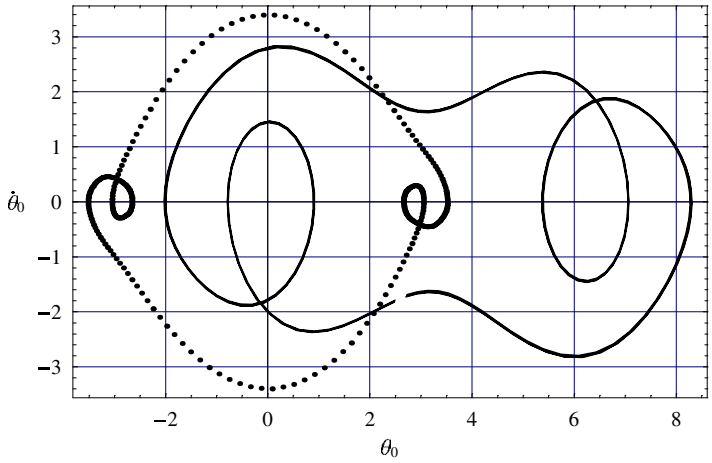

Figure 5. $a = 0.662\,5386$, $\Theta_0 = 0$, $C = \{3.762\,21,\ 1.2,\ 0.281\,255,\ 0.108\,206,\ 0.045\,3349,\ 0.019\,4243,\ 0.008\,593\}$, $\delta = \{2.832\,99,\ 2.527\,79,\ 1.718\,91\ 1.209\,19,\ 0.687\,021,\ 0.186\,016,\ -0.340\,99\}$, $\{\theta(0), \dot{\theta}(0)\} = \{-2.242\,7189, -1.945\,4008\}$.

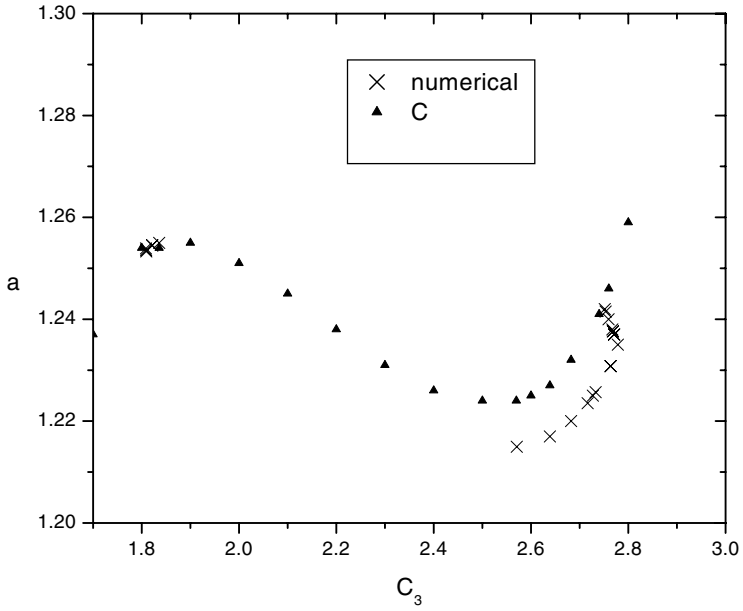

Figure 6. $\Theta_0 = 0$. All solutions of type **C** found by the present method and by direct numerical integration of the differential equation.

Three different initial conditions were taken in each case and the results were the same. Apparently, the solution does not depend on the choice of initial conditions although this may be difficult to check numerically.

For values of a between these two sets, multiple-period solutions were found (figure 9); for values of a very near each of the period-3 attractors, a double period occurred. The method is not accurate enough in order to investigate the period-doubling sequence. The motion is

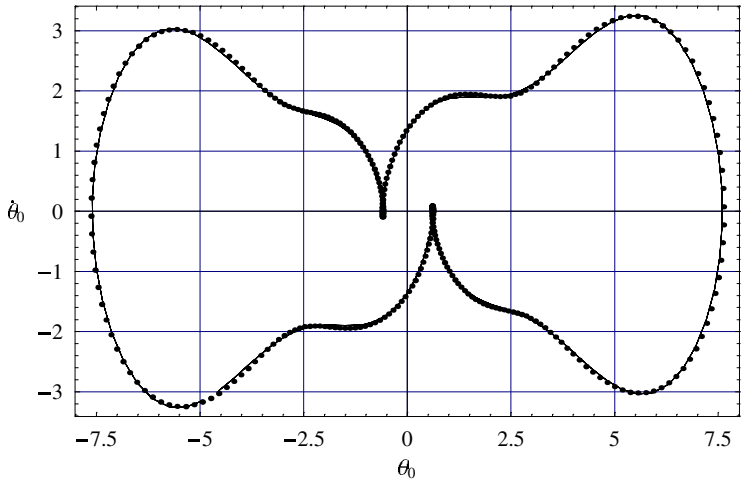

Figure 7. $a = 1.254\,056\,567$, $\Theta_0 = 0$, $C = \{5.225\,76,\ 1.83,\ 0.319\,777,\ 0.262\,712,\ 0.035\,747,\ 0.005\,615,\ 0.007\,400\}$, $\delta = \{2.056\,48,\ 2.703\,82,\ -2.580\,06,\ -1.939\,45,\ -1.3915,\ 2.971\,85,\ -2.552\,01\}$, $\{\theta(0), \dot{\theta}(0)\} = \{-4.943\,544, -3.170\,4122\}$.

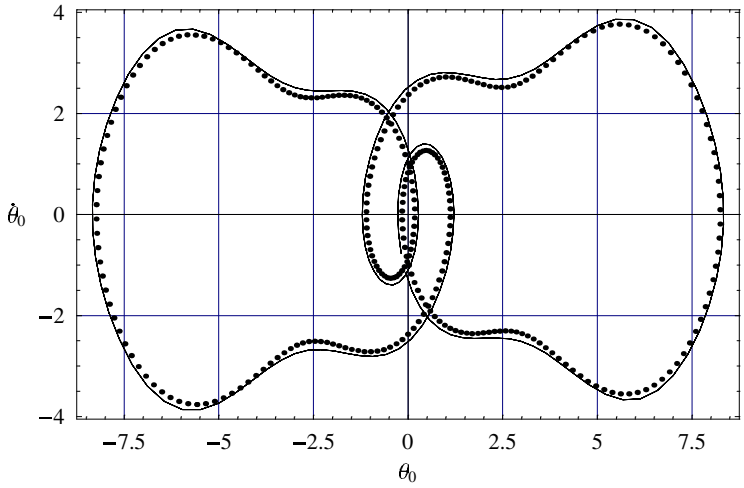

Figure 8. $a = 1.221\,602\,08$, $\Theta_0 = 0$, $C = \{5.308\,087, 2.58, 0.097\,838, 0.312\,174, 0.023\,146, 0.039\,772, 0.017\,273\}$, $\delta = \{2.0294, 2.671\,656, -2.488\,3456, -2.070\,46, -1.402\,045, 2.791\,96, -3.016\,801\}$, $\{\theta(\pi/2), \dot{\theta}(\pi/2)\} = \{0, 0\}$.

bounded, independently of initial conditions and it looks as if the solution wanders between the two stable attractors.

For $a < 1.214\,87$ or $a > 1.255$ multiple-period solutions were found and as the value of a departed from these values, the solution became complex (figures 10 and 11). The pendulum motion seems to be a totally unpredictable sequence of oscillations and gyrations.

4.1.4. Group D. Only one period-3 solution was found by the present method and plotted in figure 12. For some values of C_3, the iteration method produced a sequence of oscillatory values of the other coefficients that would not converge. No orbit has been found by

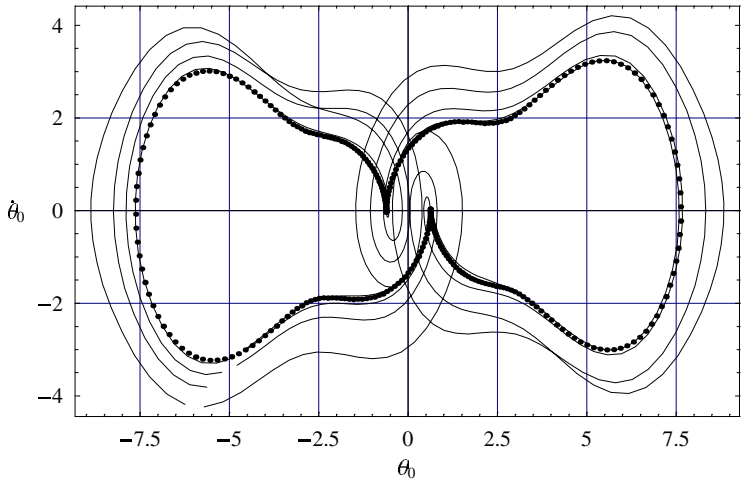

Figure 9. $a = 1.252\,312\,334$, $\Theta_0 = 0$, $C = \{5.238\,07,\ 1.8,\ 0.333\,002,\ 0.258\,393,\ 0.035\,615,\ 0.004\,971,\ 0.007\,388\}$, $\delta = \{2.058\,25,\ 2.700\,95,\ -2.575\,16,\ -1.940\,66,\ -1.386\,53,\ 2.962\,36,\ -2.533\,44\}$, $\{\theta(0), \dot{\theta}(0)\} = \{-4.937\,7366, -3.156\,7687\}$.

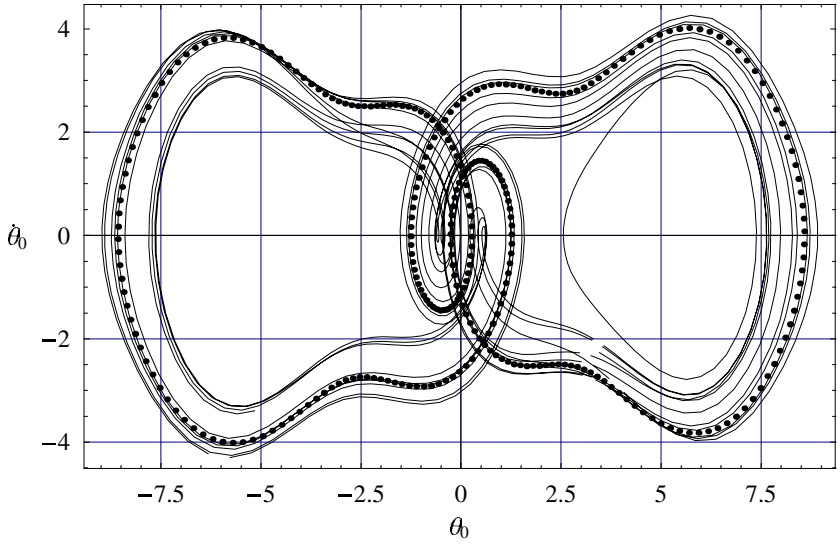

Figure 10. $a = 1.258\,5829$, $\Theta_0 = 0$, $C = \{5.527\,41,\ 2.8,\ 0.069\,445,\ 0.290\,106,\ 0.000\,285,\ 0.057\,911,\ 0.021\,754\}$, $\delta = \{2.029\,16,\ 2.663\,92,\ -2.244\,93,\ -2.084\,72,\ -0.522\,18,\ 2.746\,61,\ -3.062\,85\}$, $\{\theta(0), \dot{\theta}(0)\} = \{-5.957\,5974, -3.996\,0918\}$.

numerical integration in these regions. As one solution has been found in this group, it is very probable that very unstable orbits exist that were not detected by either analytical or numerical methods.

For other values of C_3, after a number of iterations, solutions ceased to exist. We believe that these cases were incorrectly predicted by the first order approximation.

4.1.5. Group E. Only one period-3 solution was found by numerical integration, for $a = 1.45$ (figure 13). For other a the motion has been found to be unbounded (nonoscillatory).

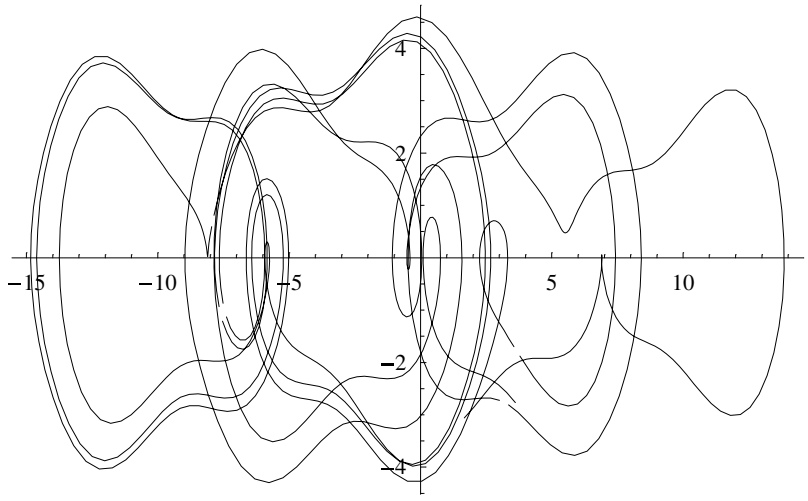

Figure 11. Numerical integration only. $a = 1.26$, $\{\theta(0), \dot{\theta}(0)\} = \{-5.957\,5974, -3.996\,0918\}$.

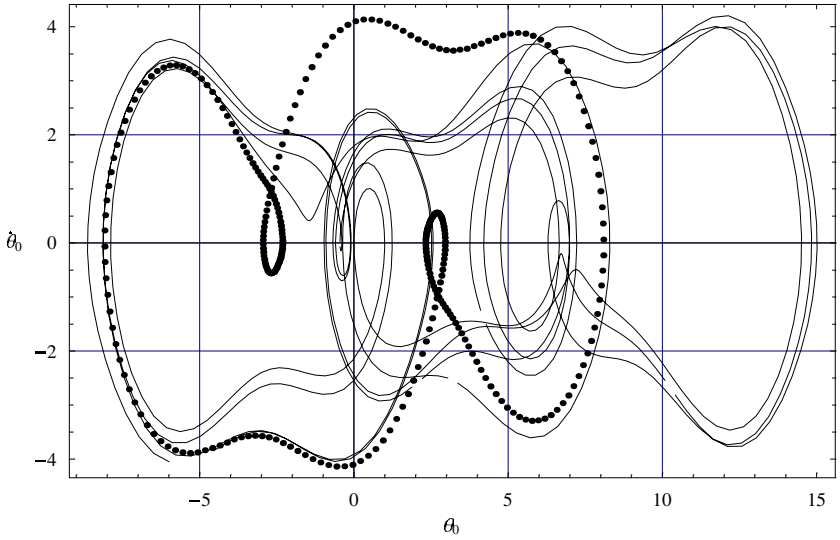

Figure 12. $a = 1.1736$, $\Theta_0 = 0$, $C = \{5.614\,74,\ 2.6,\ 0.290\,28,\ 0.184\,12,\ 0.084\,9369,\ 0.034\,9335, 0.030\,2006\}$, $\delta = \{2.433\,74, 2.632\,97, -2.918\,57, -0.962\,495, -0.668\,341, -1.780\,84, -1.960\,62\}$, $\{\theta(0), \dot{\theta}(0)\} = \{-4.586\,8348, -3.795\,5868\}$.

4.1.6. Group F. The iteration method did not converge. Also, no orbit has been found by numerical integration.

4.2. $\Theta_0 = \pi$

A similar approach has been adopted to analyse motions centred on the top position of the pendulum but we did not investigate thoroughly all the possibilities (figure 14). The iteration method did not converge most of the time.

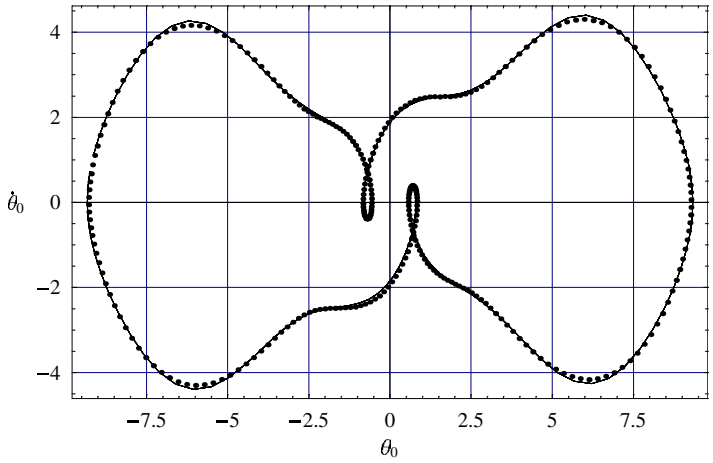

Figure 13. $a = 1.445$, $\Theta_0 = 0$, $C = \{6.5487, 2.553\,08, 0.253\,432, 0.130\,676, 0.103\,256, 0.063\,4082, 0.007\,189\,58\}$, $\delta = \{2.043\,12, 2.6856, -2.464\,72, -1.9426, 2.098\,81, 2.756\,75, -3.033\,97\}$. Numerical integration has been performed for $a = 1.45$ in order to have the same value of C_3, $\{\theta(\pi/2), \dot{\theta}(\pi/2)\} = \{0, 0\}$.

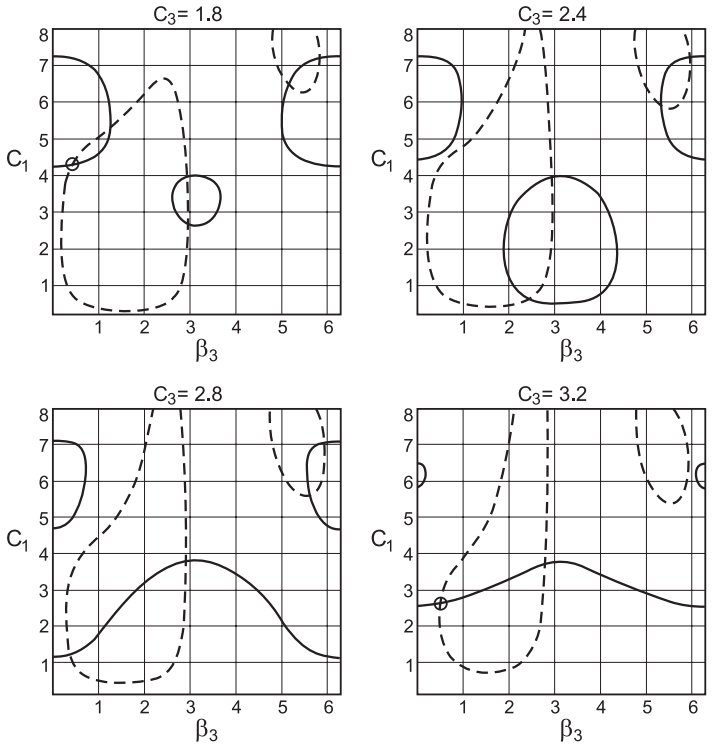

Figure 14. Same as in figure 1 for $\Theta_0 = \pi$, first order approximation. Full lines represent $g_R(C_1, \beta_3) = 0$ and broken lines represent $g_I(C_1, \beta_3) = 0$. C_1 and β_3 at the intersections are the first order solutions.

The most typical solution is shown in figure 15. This is the case reported in [2]. The solution is quite stable and apparently does not depend on initial conditions.

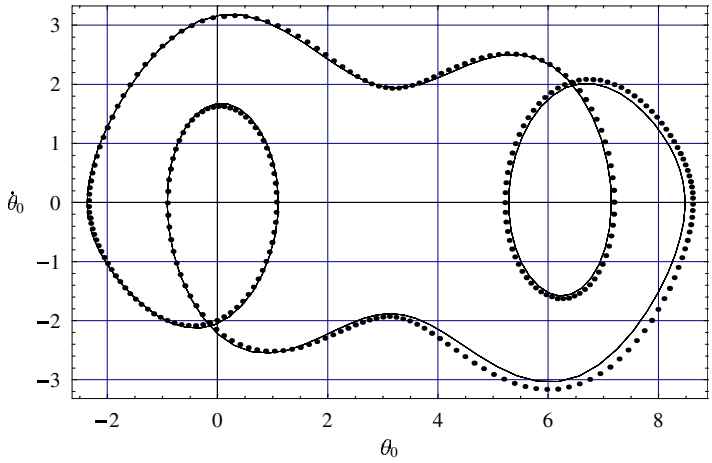

Figure 15. $a = 0.682\,2569$, $\Theta_0 = \pi$, $C = \{4.582\,35, 1.8, 0.468\,078, 0.186\,778, 0.062\,611, 0.010\,667, 0.002\,898\}$, $\delta = \{1.063\,58, 2.357\,14, 0.906\,639, -2.410\,26, -1.170\,66, -0.653\,061, 0.747\,89\}$, $\{\theta(0), \dot{\theta}(0)\} = \{-2.317\,076, -0.262\,10\}$.

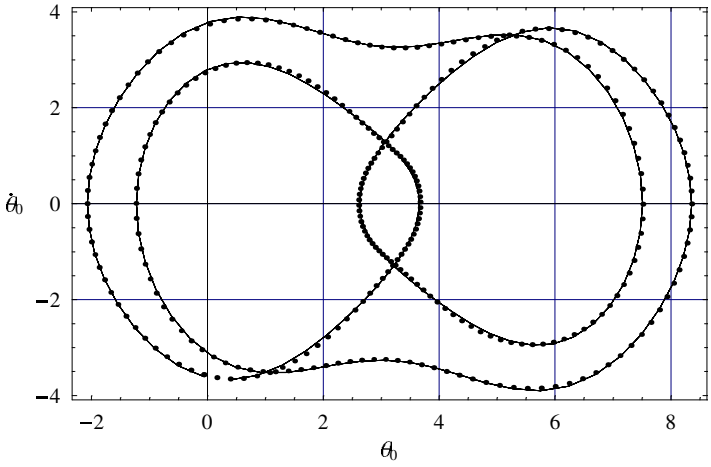

Figure 16. $a = 1.345\,29$, $\Theta_0 = \pi$, $C = \{2.391\,03, 3.26, 0.189\,671, 0.293\,506, 0.061\,083, 0.033\,2121, 0.028\,5023\}$, $\delta = \{1.1175, 2.761\,09, -2.184\,14, -3.093\,98, -0.781\,783, 1.912, 2.687\,57\}$. Numerical integration has been performed for $a = 1.3399$ in order to have the same value of C_3, $\{\theta(0), \dot{\theta}(0)\} = \{-0.050\,371\,426, -3.565\,5425\}$.

Figure 16 shows another solution. This is very unstable. Sometimes it was impossible to reproduce a solution found a week before using the same computer.

5. Conclusions

By fixing the system parameters $\epsilon = 0.2$ and $f = 0.689$, we found all period-3 attractors for values of C_3 and C_1 in the ranges $1.2 \leqslant C_3 \leqslant 3.6$ and $0.2 \leqslant C_1 \leqslant 8$. These are rather high amplitude motions and we expect them to be produced by large amplitude forces. We found, in theory, five groups of period-3 solutions centred in the potential minimum ($\Theta_0 = 0$). Numerical integration of the differential equation shows that most of them are quite unstable.

Only two of them (**A** and **C**) are reasonably stable. Therefore, only forces a within very narrow ranges produce stable p-3 motion: [0.5153, 0.521 955], [1.214 87, 1.243] and [1.2533, 1.255].

The method may fail to detect some nonstable orbits.

For oscillations around the top position $\Theta_0 = \pi$, a must be around 0.68.

When the system contains more than one periodic solution, the motion depends on the initial conditions. This is very clear for values of a around 0.52, when period-1 and period-3 solutions coexist. For a around 1.254 only one period-3 solution is found and it is independent of the initial conditions. Multiple period solutions arise for values of a outside these ranges; as a departs from attracting periodic sets the motion becomes chaotic.

This method can be extended to investigate all mode-locked solutions. If the amplitude of the driving term is small, then orbits with frequency equal to the driving frequency occur, around the minimum potential (paper I). For $\epsilon = 0.2$ and $f = 0.689$ period-1 orbits were observed for values of a up to 0.6.

As the amplitude of the drive is increased, nonlinear effects become important and period-1 orbits occur only for values of a in some narrow bands, as in period-3 cases. There is no reason to expect different kinds of results for other periodic states.

Peterson and Davidson [4] summarized their numerical investigations in a state diagram where regions of chaos, mode-locked states and complicated periodic states are mapped in terms of the driving force amplitude and its frequency. This kind of map fails to show the coexistence of many periodic states and the dependence upon the initial conditions. Some solutions are missed as numerical integration always starts from $\{\theta(0), \dot{\theta}(0)\} = \{0, 0\}$.

We suggest a state diagram, in terms of the initial conditions and force strength, where the dissipation parameter ϵ and the frequency f are kept fixed.

Appropriate initial conditions could be, for example, $\{\theta(0), \dot{\theta}(0)\} = \{0, v_0\}$, as any motion passes through the pendulum equilibrium position. This diagram would be a map in the space $v_0 \times a$. It would be formed by a wide band of a, $0 < a \lessapprox 0.6$, which gives rise to period-1 motion, many narrow stripes and islands representing large amplitude periodic motions and the respective basins of attraction. The bands can be determined by the method reported here, without great difficulty, and the values of v_0 by numerical integration.

This rather simple set-up allows direct visualization of the structure of the solutions and it may help answer the question of whether it is possible to extend our findings to all diagrams:

- The motion is stable and independent of the initial conditions wherever there is only one periodic solution.
- The period is doubled and transition to chaos may occur through a period-doubling sequence as the value of a departs from the border of some mode-locked oscillation region. Due to the extreme sensitivity of the motions to the values of a, sometimes it is very difficult to distinguish the period-doubling sequence. If there is no attracting set nearby, the solution may run to infinity, that is to say, the pendulum may rotate indefinitely.
- If, for the same set of physical parameters, there is more than one stable periodic solution, the motion is one of the solutions, depending on the initial conditions.
- A hybrid of two types of motion is observed near the borderlines of two neighbouring attracting sets in the map.

Acknowledgment

LHAM is supported by CNPq.

References

[1] Kucinski M Y and Monteiro L H A 2000 *J. Phys. A: Math. Gen.* **33** 8489
[2] Blackburn J A 1989 *Rev. Sci. Instrum.* **60** 422
[3] D'Humieres D *et al* 1982 *Phys. Rev.* A **26** 3483
[4] Pedersen N F and Davidson A 1981 *Appl. Phys. Lett.* **39** 830
[5] Kerr W C *et al* 1985 *Z. Phys.* B **59** 103
[6] Heng H *et al* 1994 *Int. J. Bifurcation Chaos* **4** 751
[7] Rasband S N 1990 *Chaotic Dynamics of Nonlinear Systems* (New York: Wiley)